*Journal of Applied Fluid Mechanics*, Vol. 18, No. 3, pp. 809-820, 2025.
Available online at www.jafmonline.net, ISSN 1735-3572, EISSN 1735-3645.
https://doi.org/10.47176/jafm.18.3.2768

# Numerical Investigation of Impinging Planar Shock Wave Interaction with Axisymmetric Slender Body

M. A. Ali and P. Mondal†

*Department of Space Engineering and Rocketry, Birla Institute of Technology, Mesra, Ranchi, 835215, India*

†*Corresponding Author Email: pmondal@bitmesra.ac.in*

## ABSTRACT

Shock Wave Boundary Layer Interactions represent a complex flow feature combining high-speed inertial force - dominated flows with low-speed viscous force dominated regions. In this research, planar oblique shock impingement on finned missile body (slender body) have been studied, involving a complex flow field of shocks and expansion waves. Computational studies are used to perform quantitative and qualitative analysis of multi body configurations and investigate the associated flow physics. There is change in induced forces and moments of finned body with change in location of shock impingement, due to the combined effect of enhanced compression, expansion and flow pitch angle on different regions of the missile. For fixed lateral separation between the bodies, changes in coefficient of forces and moments of missile body are very small for shock impingement locations close to fin leading edge. The fins contribute about 50-60% to coefficient of forces and moments of finned missile body. With change in angle of incidence, there is change in polarity of forces and moments illustrating extreme sensitivity of missile body to location of shock impingement, which is due to the combined effect of enhanced compression and expansion on different regions of the missile.

***Article History***

*Received April 8, 2024*
*Revised July 26, 2024*
*Accepted September 21, 2024*
*Available online January 1, 2025*

***Keywords:***

*Shock wave*
*Boundary layer*
*Finned missile body*
*Shock impingement*
*CFD*

## 1. INTRODUCTION

Shock Wave Boundary Layer Interactions (SWBLIs) have become the focus of scientific study since the conception of early high-speed vehicles. They represent a complex flow feature combining inertial-dominated high-speed flows with viscous dominated low-speed regions. The result is often an adverse thickening of the boundary layer with associated fluctuations in pressure and temperature which can be detrimental to vehicle performance and its safety. In high speed flows, the presence of multiple bodies in close proximity leads to development of complex interference flow field like the case of a supersonic intake where the incoming air is compressed by the oblique shocks, which include boundary layer interaction on the opposite or adjacent surfaces. Likewise, shock waves which are originated from nose of the aircraft or leading edge of the wing can impinge on the stores released from the aircraft leading to a complex interference flow field of impinging shock and expansion waves. Axisymmetric body like missile often have blunt projections in the form of protrusions or control surfaces known as fins on the external surface in order to accommodate some aerodynamic and control component. The presence of fins induces shocks causing SWBLI in near vicinity which affect the control forces and moments generated by missile.

Studies related to Shock Wave Boundary Layer Interactions were mostly related to flat plate, lately the effect of curved surface on SWBLIs have been investigated. Brosh et al. (1985) investigated the oblique shock wave impingement on a circular cylinder in supersonic flow of Mach number 3.0. Tutty et al. (2002) studied the viscous flow over a long thin cylinder numerically. Sawchuk and Zamir (1992) investigated numerically the axial flow over the outer surface of a circular cylinder. Gai and Teh (2000) investigated the interaction between conical shock wave and 2-D turbulent boundary layer over flat plate at Mach 2. Kussoy et al. (1980) studied the complex flow features of a 3-D shock wave impingement on an axisymmetric boundary layer. Alvi and Settles (1992) discussed the flow physics of SWBLIs where the shock was generated with a fin. Dolling (2001) reviewed the weakness in physical understanding of SWBLIs and made some suggestions in near term. Knight et al. (1987) investigated experimentally as well as theoretically the supersonic flow over a sharp fin at Mach number of 3. Zheltovodov (1982) studied the 3-D SWBLIs on a flat

**NOMENCLATURE**

| | | | |
|---|---|---|---|
| L | body length | Φ | body azimuthal angle |
| D | base diameter | $\Delta C_n$ | normal force interference load |
| c | fin chord length | $\Delta C_a$ | axial force interference load |
| b | fin half span | x’ | axial location of shock impingement |
| t | max fin thickness | $\Delta C_p$ | pressure coefficient difference from isolated |
| $x_{LE}$ | axial distance from body leading edge to fin leading edge | $x_{CP}$ | axial location of centre of pressure |
| α | angle of attack | $x_{CG}$ | axial location of centre of gravity |
| Δx | axial separation between body leading edge and shock generator leading edge | $y_f$ | spanwise distance from fin root |
| Δy | lateral separation between body leading edge and shock generator leading edge | $\Delta C_{n,body}$ | body contribution to normal force coefficient |
| y+ | non-dimensional boundary layer coordinate | $\Delta C_{n,fin}$ | fin contribution to normal force coefficient |
| $C_p$ | coefficient of pressure | $\Delta C_{m,body}$ | body contribution to pitching moment coefficient |
| $C_n$ | coefficient of normal force | $\Delta C_{m,fin}$ | fin contribution to pitching moment coefficient |
| $C_a$ | coefficient of axial force | $C_{p,upper}$ | coefficient of pressure on fin upper surface |
| $C_m$ | coefficient of pitching moment | $C_{p,lower}$ | coefficient of pressure on fin lower surface |

surface. Cenko and Waskiewicz (1983) demonstrated a unique method to predict store aerodynamic characteristics in aircraft flow field with the help of force and moment influence functions obtained from wind tunnel test by traversing the store through oblique shock generated by a wedge or an inclined plane. Waskiewicz et al. (1983) demonstrated the capability of aerodynamic panel method to predict aerodynamic characteristics of store in near proximity of an oblique shock generated by a flat plate at an angle of attack. Newman et al. (1992) investigated the store separation from a hypersonic vehicle with 6 DOF analysis. Wilcox (1995) experimentally studied the aerodynamics of two store models above a flat plate at hypersonic Mach number of 6. Chaplin et al. (2011) investigated the aerodynamics of slender bodies at high-speed flow experimentally and numerically. Robertson et al. (2015) explored the effect of impingement of planar shock wave on the aerodynamics of a tangent ogive cylinder by numerical and experimental methods in supersonic flow. Stephen et al. (2013) confirmed the presence of shock induced horse shoe vortices by studying the impingement planar shock wave on an ogive cylinder at Mach number of 3. Pickles et al. (2016, 2017) investigated the SWBLIs on an axisymmetric cylindrical body. To study the evolution of vortex structures more accurately, higher-order turbulence models Jin and Kuznetsov (2024) or direct numerical simulation Ijas et al. (2024) can be used for the flow calculation.

In SWBLIs, due to the shock wave impingement on the axisymmetric slender body (missile) and the one induced due to the fins of the missile in tandem could drastically affect the aerodynamic characteristics of the missile depending on the shock strength, angle of incidence and location of shock impingement. The goal of this research work is to quantify the induced forces and moments due to multiple SWBLIs and to understand the associated flow physics.

## 2. MTHODOLOGY

### 2.1 Description of Test Models and Configuration

The present test model is taken as a tangent ogive cylinder with length of forebody as 2.5D and cylindrical afterbody with a slenderness ratio (L/D) of 6, where base diameter of the missile (D) is 11mm. Missile with sharp fins had cruciform control fins of hexagonal profile (0.3c-0.4c-0.3c) with chord of the fins (c) equal to 11mm i.e. c/D = 1, semi-span length (b) of 7.15mm i.e. b/D = 0.65 and thickness/chord (t/c) equal to 0.1. These fins were positioned on the missile with its leading edge at $x_{LE}/D = 5$. Oblique shock is generated with the help of a shock generator which is double wedge-shaped with half angle of $10^{\circ}$ and a maximum thickness of 10mm. Schematic representation of test model and shock generator are shown in Fig. 1 and Fig. 2 respectively.

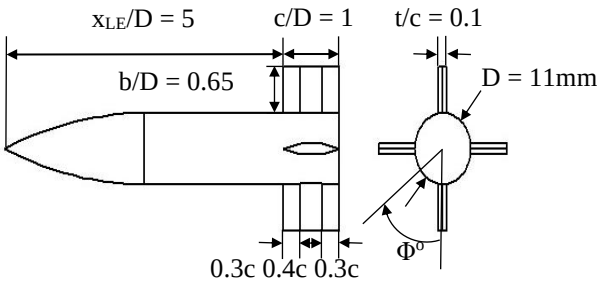


**Fig. 1 Finned missile body**

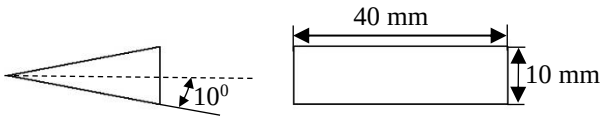


**Fig. 2 Shock generator**

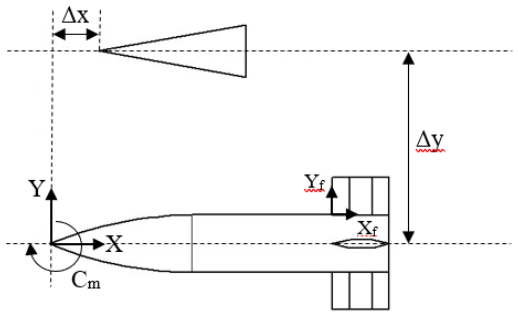


**Fig. 3 Positive sign convention of axial separation, lateral separation and pitching moment**

For multi-body test configuration, axial separation (Δx) and lateral separation (Δy) between the bodies were altered to change the position of shock impingement. Axial separation (Δx) is the location of leading edge of shock generator relative to missile nose in x-direction and lateral separation (Δy) is the location of leading edge of shock generator relative to missile nose in y-direction as shown in Fig. 3. In this study, lateral separation (Δy) was kept constant and axial separation (Δx) was varied with shock impingement location close to fins. The coefficient of moment for the missile body was calculated with respect to the nose of missile body.

### 2.2 Solver Description

Computational analysis of all test configurations was carried out using ANSYS Fluent, for Reynolds number of $2.78 \times 10^5$ and Mach number of 2, by solving Reynolds Averaged Navier Stokes (RANS) equations under steady, implicit solver scheme. To simulate the turbulent flow, turbulence model was taken as the Menter's k-ω SST. Ideal gas condition and viscosity based on Sutherland law were selected as fluid properties. Courant Number was set as 1 for all computations. Flow discretization was done using second order upwind scheme. First order upwind scheme was used for discretization of the model equations.

### 2.3 Grid Generation

All 3D grids for computation were created with the help of Pointwise v18.3 (2019) using near-wall treatment. Computational domain is taken only half of the complete flow-field since all test configurations were symmetric about XY plane at origin. The far-field boundary distances at upstream and downstream directions are 1D and 3D respectively, where D is the base diameter of missile. Height of the domain was adjusted to contain the shocks emanating from shock generator and missile body.

To resolve the boundary layer on the wall sufficiently, first layer of grid spacing over the shock generator and missile body was set as 0.001mm to ensure y+ value of the order of unity. Boundary layer resolution over the missile body was done using 25 cells with a growth ratio of 1.3. Resultant 3D mesh for isolated body and multi-body configuration consisted of 1.04 million and 1.45 million cells respectively, which is shown in Fig. 4.

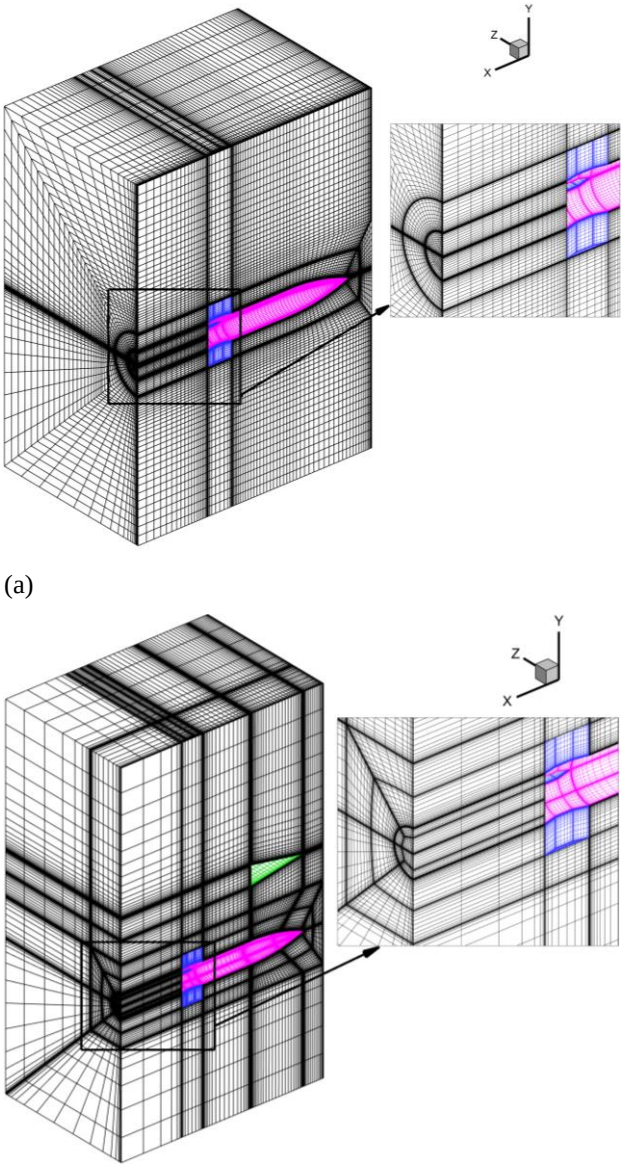


**Fig. 4 Computational domain for (a) Isolated body and (b) Multi-body arrangement**

### 2.4 Boundary Conditions

Inlet and Farfield boundaries were defined as Pressure-Farfield type at static pressure of 26428.15 Pa, static temperature of 166.67 K and Mach number of 2. Outlet was defined as Pressure-Outlet type which involves calculation of flow properties by extrapolating results from upstream, for a supersonic flow ANSYS Fluent (2020). All the surfaces of models of interest were given no-slip adiabatic wall boundary condition and remaining boundaries were given the symmetric boundary condition.

## 3. RESULTS AND DISCUSSION

Multi body configuration of Robertson et al. (2015) was used to validate the current computational setup.

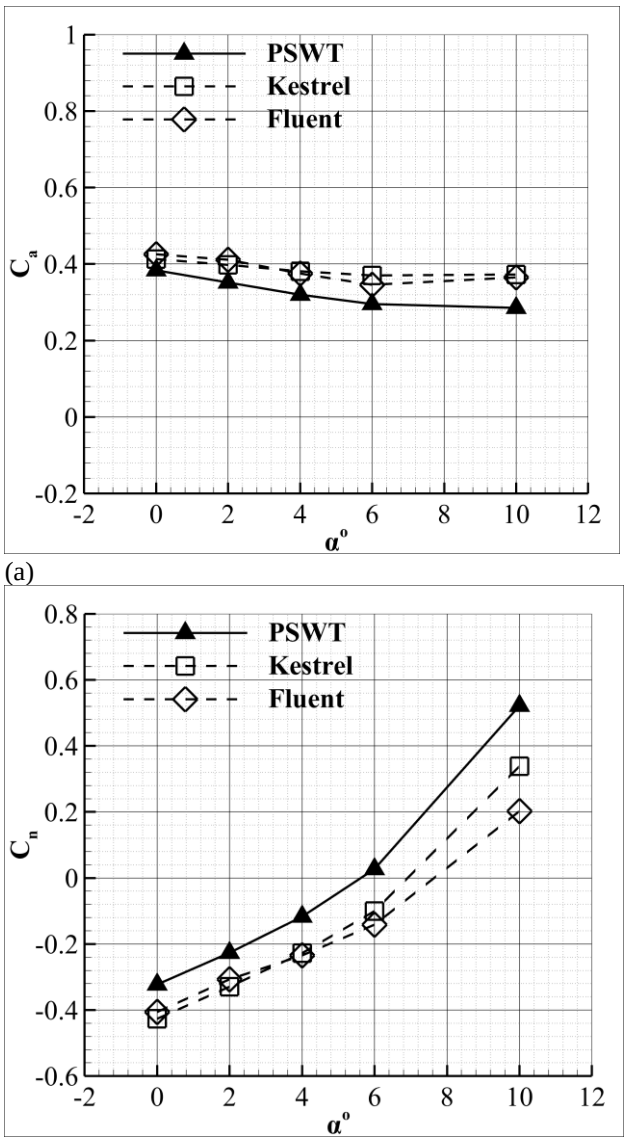


**Fig. 5 Variation in (a) coefficient of axial force and (b) coefficient of normal force, with angle of attack ($\alpha^o$)**

Experiments were carried out at Mach 2 in the FSU polysonic wind tunnel (PSWT) and numerical investigations using the Kestrel multi-physics flow solver Robertson et al. (2015). Comparison of axial and normal force coefficients for different angles of attack (α) obtained by Robertson et al. (2015) and those obtained using current computational setup is shown in Fig. 5 (a) and Fig. 5 (b) respectively.

Present computational setup captures the aerodynamic trend well as seen in the experiments and simulations of Robertson et al. (2015). The offset between the PSWT and the present Fluent result at higher angle of attack is due to the use of RANS model in highly separated flows and the absence of model holding sting in present simulations.

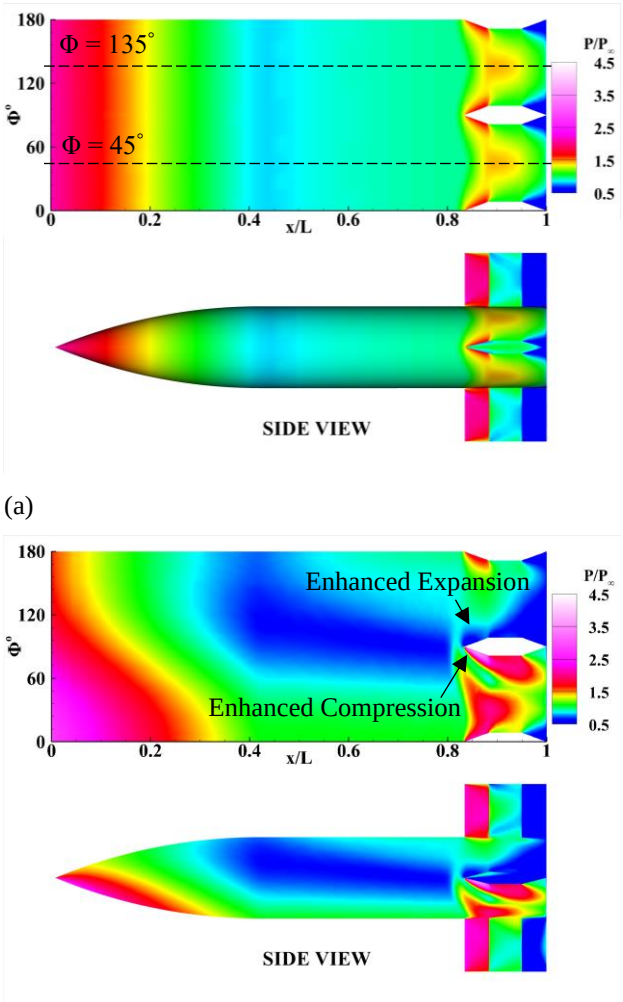


**Fig. 6 Surface pressure contour on finned missile body at (a) α = 0° and (b) α = 10°**

### 3.1 Aerodynamics of Isolated Finned Missile Body

#### 3.1.1 Flow Features of Isolated Finned Missile Body

In supersonic regime, the presence of sharp fins on missile body leads to a leading edge shock structure which influences the surface pressure of the fins and inter-fin region. The fins are positioned at Φ = 0°, 90°, 180°and 270° on the body. Surface pressure contours of finned missile body for α = 0° and α = 10° are shown in Fig. 6.

When α = 0°, the strength of the shocks generated by the lifting fins located at Φ = 90°, 270° are equal, which intersect with the shocks generated by the normal fins located at Φ = 0°, 180°. At α = 10°, the shock at lower side of the lifting fin is stronger than at the upper side. This results in increased pressure in lower inter-fin region and decreased pressure in upper inter-fin region as shown in Fig. 7. The effect of angle of attack on circumferential pressure distribution of finned missile body is shown in Fig. 8.

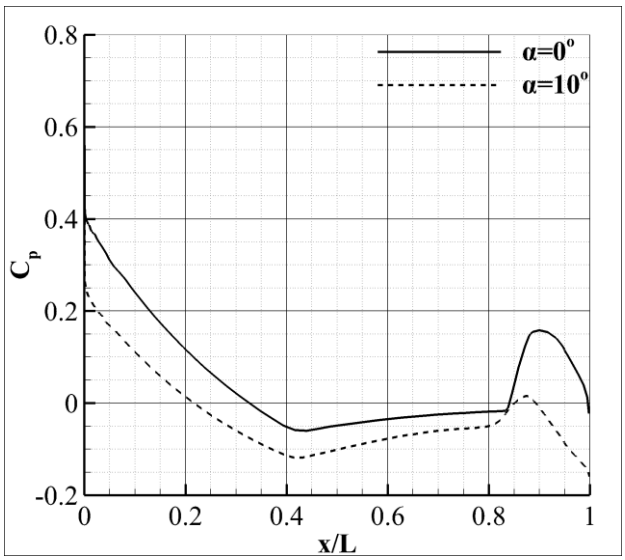


(a)

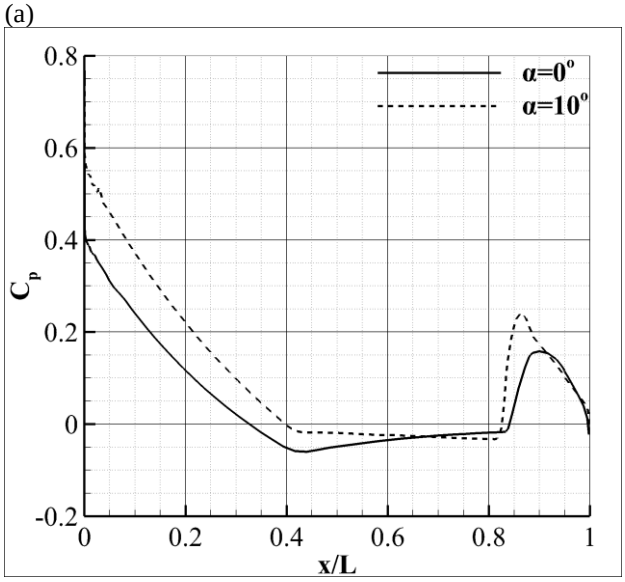


(b)

**Fig. 7 Axial pressure distribution of finned missile body on (a) nearside (Φ = 135°) and (b) farside (Φ = 45°)**

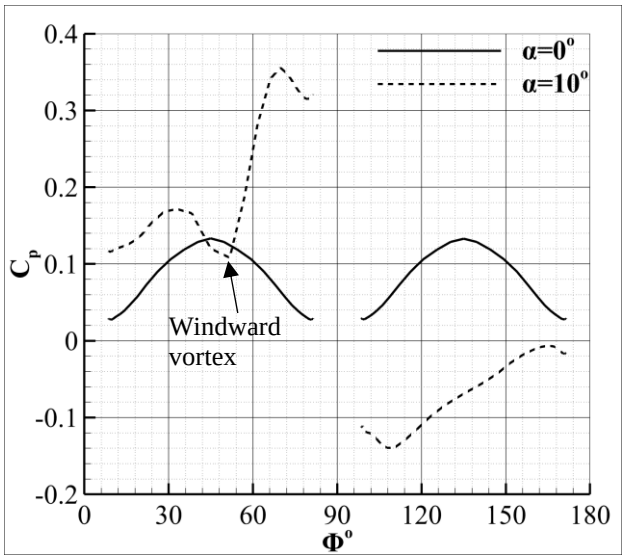


**Fig. 8 Circumferential pressure distribution at x/D = 5.64**

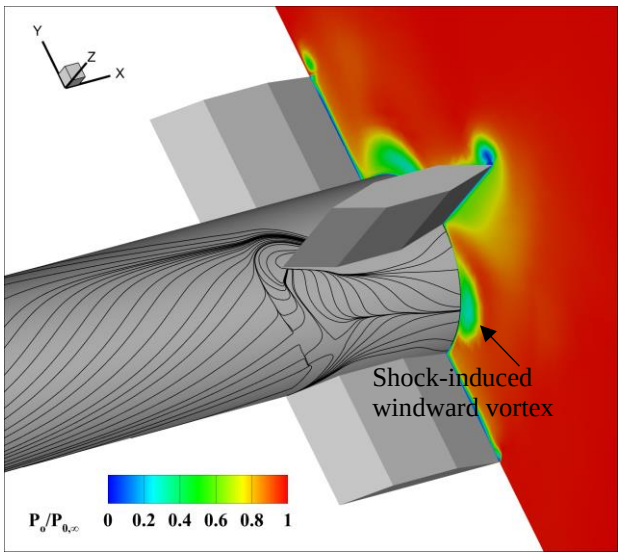


**Fig. 9 Total pressure contour on cross flow slice at x/L = 1, α = 10°**

**Table 1 Coefficients of force and moment at different angles of attack**

| | α = 0° | | | α = 10° | | |
|---|---|---|---|---|---|---|
| | $C_n$ | $C_a$ | $C_m$ | $C_n$ | $C_a$ | $C_m$ |
| Body | 0 | 0.203 | 0 | 0.823 | 0.201 | -2.438 |
| Fin | 0 | 0.292 | 0 | 0.746 | 0.292 | -3.963 |
| Total | 0 | 0.495 | 0 | 1.569 | 0.493 | -6.401 |

At α = 0°, the circumferential pressure distribution at x/D = 5.64 is similar due to equivalent shock strength in lower and upper inter-fin regions, but at α = 10°, there is a suction peak lower inter-fin region due to the presence of shock induced windward vortex as shown in Fig. 9.

### 3.1.2 Forces and Moments of Isolated Finned Missile Body

Force and moment coefficients of isolated finned missile body at different angle of attack is tabulated in Table 1. Contribution of fins to the normal force is approximately 47% and to pitching moment is approximately 60%. Change in forces and moments with change in angle of attack is due to difference in shock footprint of upper and lower inter-fin regions.

The centre of pressure for isolated finned missile body is at $x_{CP}/D \approx 5$, which remains approximately fixed for α = 0° and α = 10°. The finned missile body is statically stable and has a positive static margin as the location of centre of pressure is aft of the location of the centre of gravity ($x_{CG}/D = 4.55$).

### 3.2 Effect of Axial Stagger on Aerodynamics of Finned Missile Body

Multi-body configuration of Δx/D = 0, Δy/D = 3.36 at α = 0° was modeled using three different grids to check dependence of solution on grid size. Details related to the simulations are shown in Table 2. There is not much change in coefficient of normal force ($C_n$) with increase in mesh density. This configuration is used to know the impact of shock impingement on aerodynamics of finned missile body and then the effect of shock impingement

**Table 2 Grid independence test**

| | Grid Size | Coefficient of normal force (Cn) |
|---|---|---|
| Grid 1 | 1.86 x $10^6$ | -1.0986 |
| Grid 2 | 1.55 x $10^6$ | -1.0958 |
| Grid 3 | 1.45 x $10^6$ | -1.0950 |

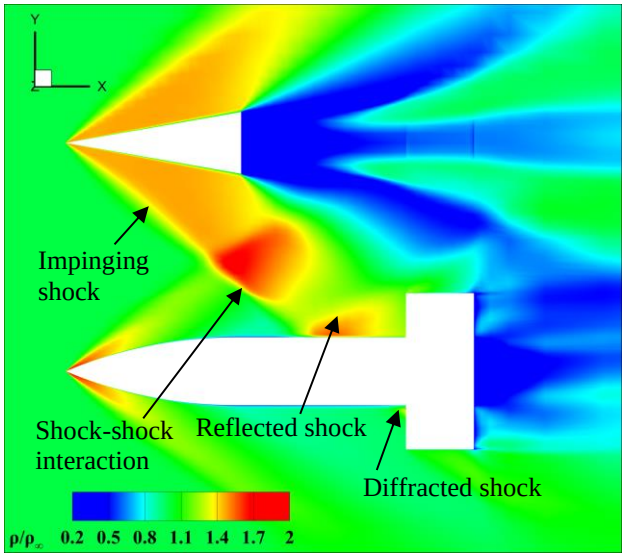


**Fig. 10 Density contour on X-Y plane for multi-body configuration of Δx/D = 0, Δy/D = 3.36, α = 0˚**

location is understood for three different axial separations (Δx/D = 0, 0.45, 0.91) and constant lateral separation (Δy/D = 3.36) with α = 0˚.

### 3.2.1 Aerodynamics of Multi-Body Configuration (Δx/D = 0, Δy/D = 3.36)

The flowfield structure associated with the multi-body configurations can be highly complex consisting of shocks and expansion waves as shown in Fig. 10. There is an interaction between shock emanating from missile body and shock generator. A part of the shock impinging on the missile body reflects off the surface and the other part diffracts around it.

Surface pressure contour on finned missile for isolated and multi-body configuration is shown in Fig. 11. Shock impingement alters the surface pressure distributions of lower and upper inter-fin regions. It is observed that there exist enhanced compression in upper inter-fin region and expansion in lower inter-fin region as the outcome of variation in flow pitch angle due to shock impingement. Presence of diffracted shock increases the pressure in lower inter-fin cancelling the effect of expansion leading to low strength compression.

Figure 12 shows the impact of shock impingement on axial pressure distribution of nearside (Φ = 135˚) and farside (Φ = 45˚). The shock impinges on nearside of finned missile body at approximately x'/L=0.65 and alters local flow pitch angle. The negative flow pitch makes a higher positive differential pressure $\Delta C_{p,near} \approx$ 0.225 on the upper inter fin region in comparison to isolated configuration of finned missile body. There is an

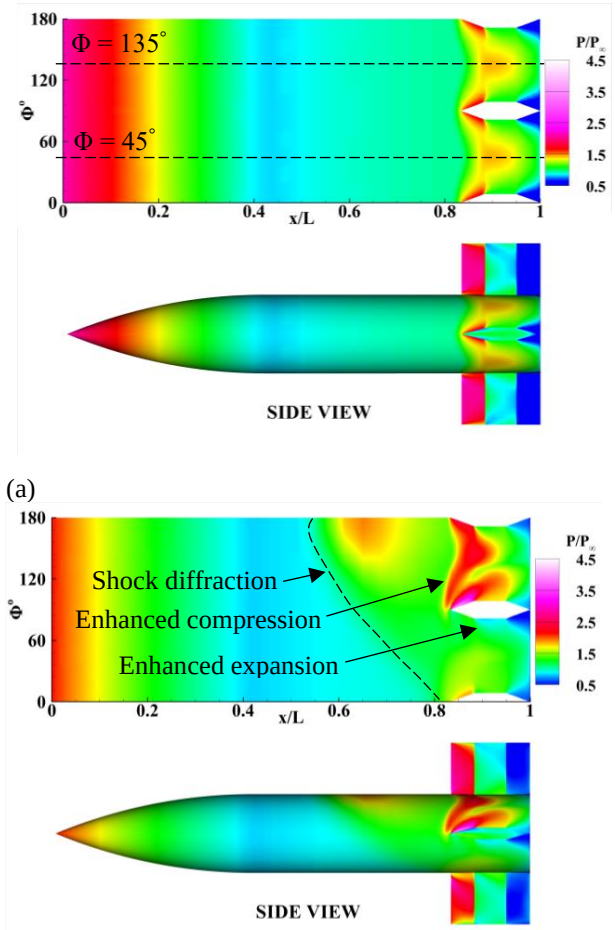


**Fig. 11 Surface pressure contour on finned missile body for (a) Isolated, α = 0˚ and (b) Multi-body configuration, Δx/D = 0, Δy/D = 3.36, α = 0˚**

increase in farside pressure of $\Delta C_{p,far} \approx 0.05$ as a result of presence of diffracted shock which cancels the effect of flow pitch angle.

Figure 13 shows the effect of negative flow pitch angle on upper inter-fin region (Φ > 90˚) and lower inter-fin region (Φ < 90˚) at x/D = 5.64. The local pressure in the regions of inter-fin surface close to the fin upper surface is further increased by the impinging shock compression footprint as seen in Fig. 12(a). There is little change in local pressure of the lower inter-fin region because the diffracted shock cancels the effect of negative flow pitch, as specified earlier, bringing the pressure distribution close to that of isolated body as seen in Fig. 12(b). These flow features affect the interference loads acting on finned missile body for multi-body configuration differentiating it from the isolated body configuration. The resulting flow features for a multi-body configuration is sensitive to the location of shock impingement.

### 3.2.2 Effect of Axial Stagger for Fixed Lateral Stagger (Δy/D = 3.36)

Figure 14 shows the surface pressure contours on finned missile body at α = 0˚ for three different axial

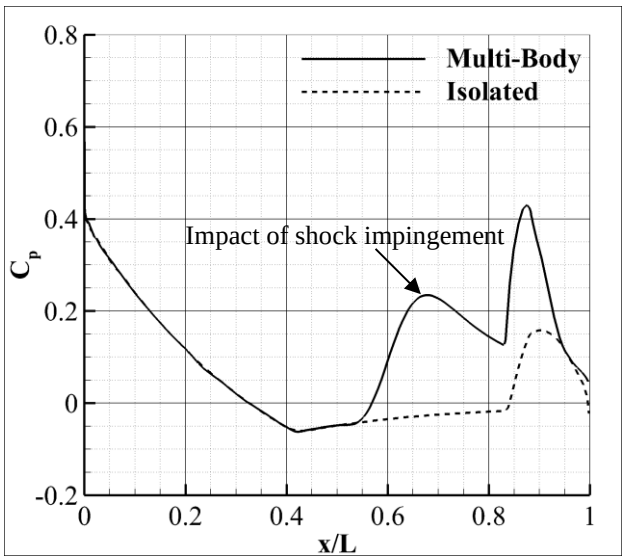


(a)

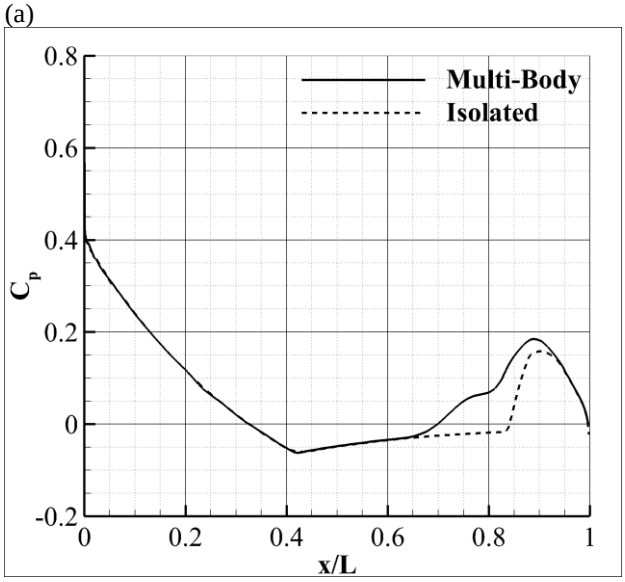


(b)

**Fig. 12 Axial pressure distribution of finned missile body (a) nearside (Φ = 135˚) and (b) farside (Φ = 45˚) for multi-body configuration, Δx/D = 0, Δy/D = 3.36, α = 0˚**

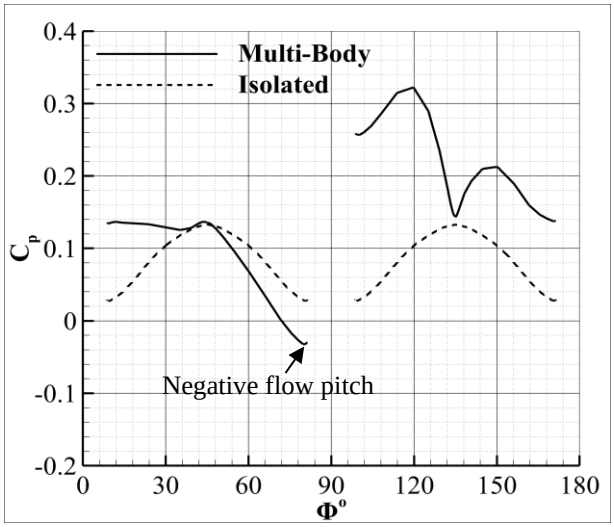


**Fig. 13 Circumferential pressure distribution at x/D = 5.64 for multi-body configuration, Δx/D = 0, Δy/D = 3.36, α = 0˚**

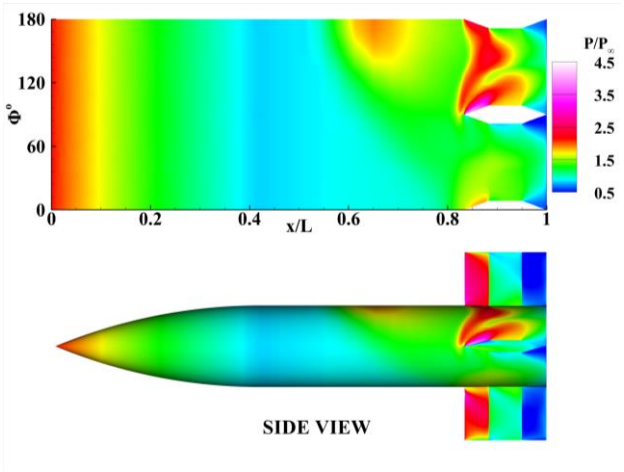


(a)

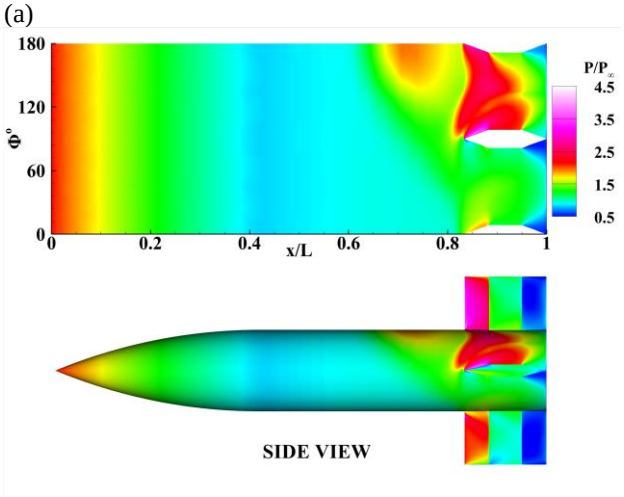


(b)

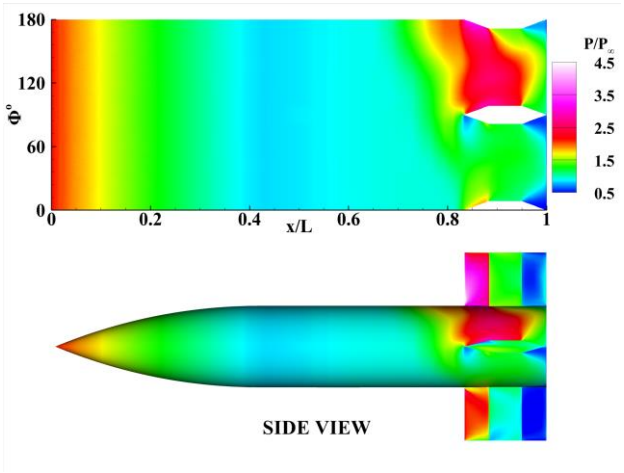


(c)

**Fig. 14 Surface pressure contour on finned missile body with lateral stagger (Δy/D = 3.36), angle of attack (α = 0˚) and axial stagger of (a) Δx/D = 0, (b) Δx/D = 0.45 and (c) Δx/D = 0.91**

separation (Δx/D = 0, 0.45, 0.91) and constant lateral separation (Δy/D = 3.36). For shock impingement much closer to fin, there is subsequent enhancement of compression in upper inter-fin region. For Δx/D =0.91,

**Table 3 Contribution of fins to the coefficients normal force and pitching moment for Δy/D = 3.36, α = 0°**

| Δx/D | Normal Force($\Delta C_n$) | | | Pitching Moment($\Delta C_m$) | | |
|---|---|---|---|---|---|---|
| | Body | Fins | Total | Body | Fins | Total |
| 0 | -0.523 | -0.541 | -1.064 | 2.325 | 2.869 | 5.194 |
| 0.45 | -0.573 | -0.609 | -1.182 | 2.784 | 3.269 | 6.053 |
| 0.91 | -0.524 | -0.571 | -1.095 | 2.691 | 3.103 | 5.794 |

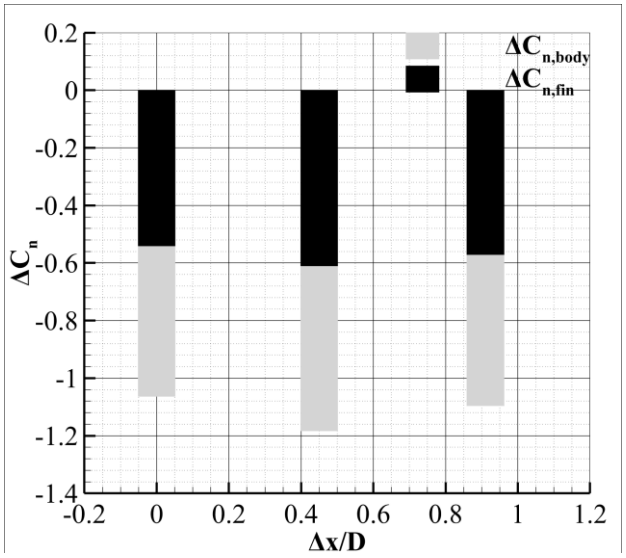


**Fig. 15 Contribution of fins and missile body to normal force coefficient, Δy/D = 3.36, α = 0°**

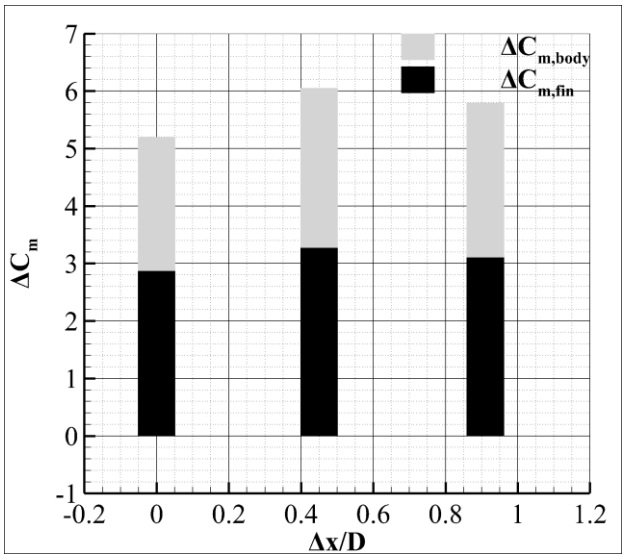


**Fig. 16 Contribution of fins and missile body to pitching moment coefficient, Δy/D = 3.36, α = 0°**

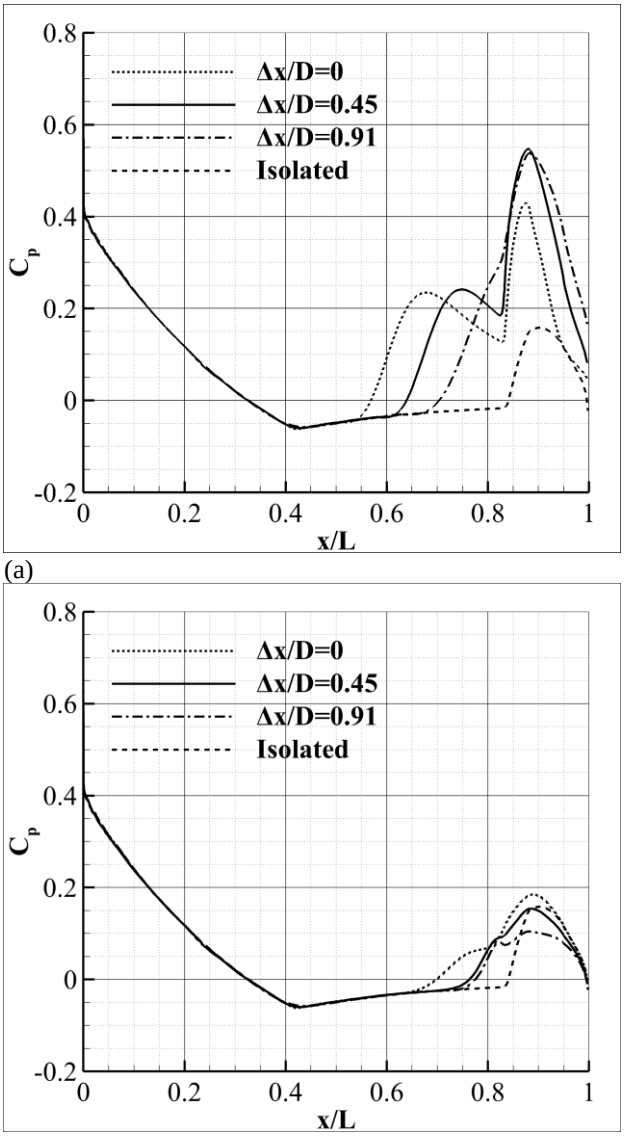


**Fig. 17 Axial pressure distribution of finned missile body (a) nearside (Φ = 135°) and (b) farside(Φ = 45°), Δy/D = 3.36, α = 0°**

there is much greater enhancement of expansion in lower inter-fin region due to flow pitch effect.

Contributions from the missile body and fins to loads is given in Table 3. The contribution in interference loads of the fin is more than half for total normal force and pitching moment as shown in Fig. 15 and Fig. 16 respectively. Fins contribution to coefficient of normal force and coefficient of pitching moment is approximated as 50% and 55% respectively. Pitching moment coefficient of missile body is positive for all configurations stating that missile is statically unstable.

The location of shock impingement impact the surface pressure distribution of nearside (Φ = 135°) and farside (Φ = 45°) as shown in Fig. 17. For Δx/D = 0.45, there is slightly higher pressure on the upper inter-fin region which results in lower normal force coefficient in comparison to other configurations. There is an increase of $\Delta C_{p,near} = C_{p,near} - C_{p,near,iso} \approx 0.4$ due to collective influence of flow pitch and shock impingement. For Δx/D = 0.91, shock impinges on the fin which leads to least influence of diffracted shock on pressure distribution of farside (Φ = 45°). Different pressure distributions for different multi-body configurations states that the resultant pressure distribution depends not

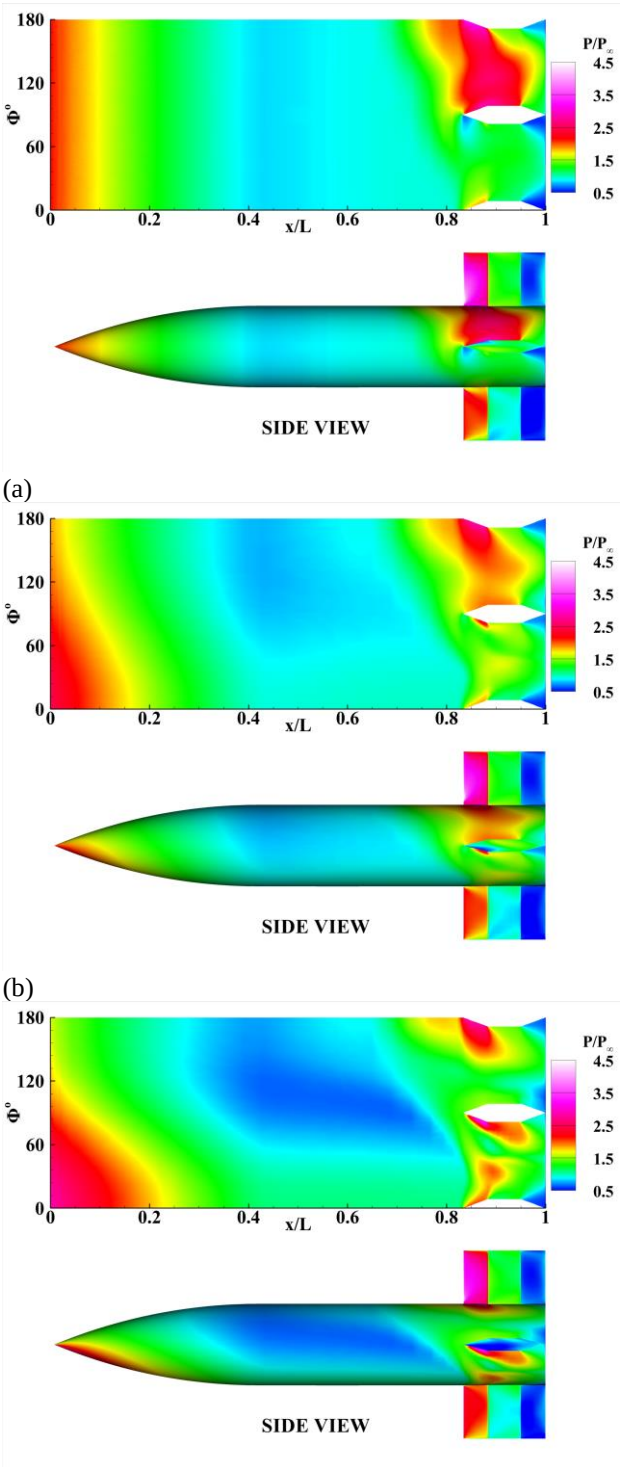


(a)

(b)

(c)

**Fig. 18 Surface pressure contour on finned missile body with lateral stagger (Δy/D = 3.36) and axial stagger (Δx/D = 0.91) at angle of attack (a) α = 0˚, (b) α = 5˚ and (c) α = 10˚**

only on location of shock impingement but also on how the diffracting shock alters the flow pitch upstream of the fins.

### 3.2.3 Effect of Angle of Incidence for Fixed Lateral Stagger (Δy/D = 3.36) and Axial Stagger (Δx/D = 0.91)

Figure 18 shows the surface pressure contours on finned missile at different angles of attack (α = 0˚, 5˚ and

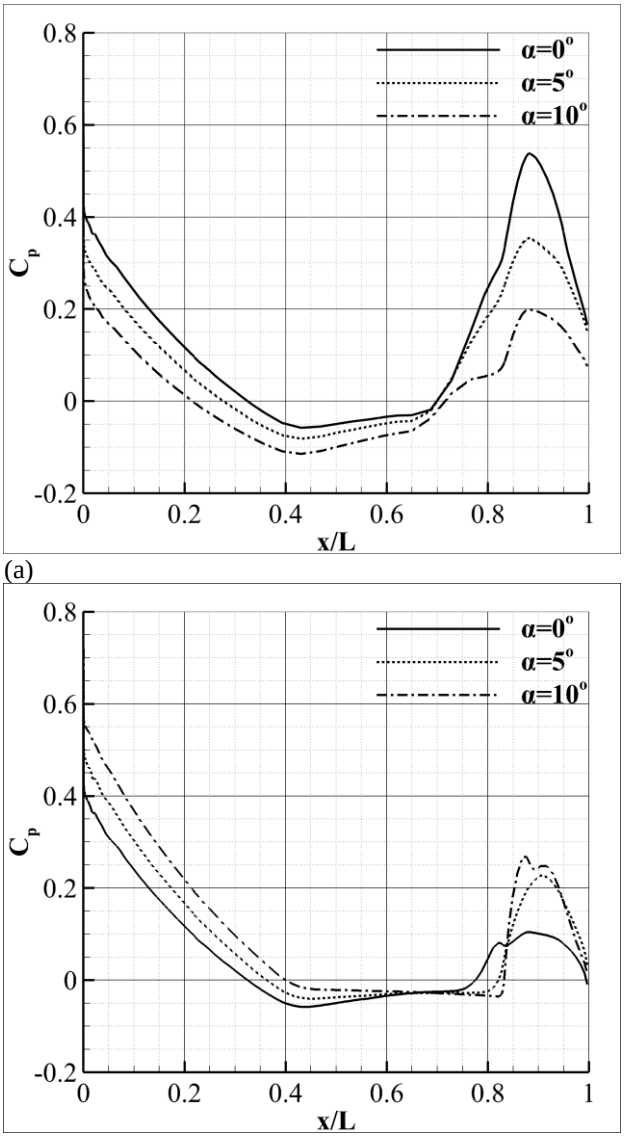


(a)

(b)

**Fig. 19 Axial pressure distribution of finned missile body (a) nearside (Φ = 135˚) and (b) farside (Φ = 45˚), Δy/D = 3.36, Δx/D = 0.91**

10˚) for constant axial separation (Δx/D = 0.91) and constant lateral separation (Δy/D = 3.36).

With increase in angle of attack of missile, there is change in shock structure of both upper inter-fin region and lower inter-fin region due to change in location of shock impingement, which consecutively influences the path of diffracted shock and the local flow pitch angles. The surface pressure distribution of nearside (Φ = 135˚) and farside (Φ=45˚) is shown in Fig. 19.

The effect of angle of attack on circumferential pressure distribution of finned missile body is shown in Fig. 20. At α = 5˚ and 10˚, there is a suction peak in lower inter-fin region due to the presence of shock induced windward vortex. The other suction peak in the upper inter-fin region corresponds to a primary vortex as shown in Fig. 21.

At the leading edge of the fin, there is an effective pressure change of $\Delta C_{p,fin} = C_{p,upper} - C_{p,lower} \approx 1$ for α =

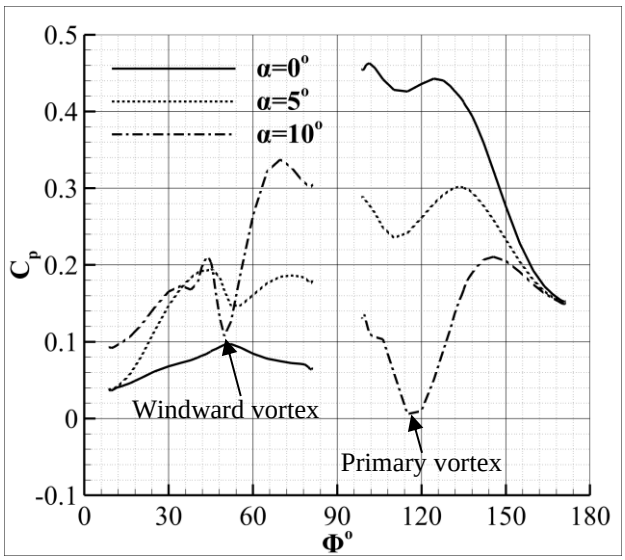


**Fig. 20 Circumferential pressure distribution of finned missile at x/D = 5.64, Δx/D = 0.91, Δy/D = 3.36**

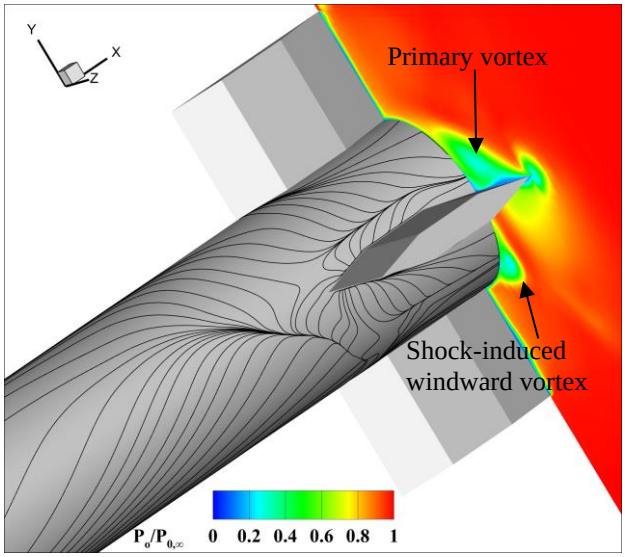


**Fig. 21 Total pressure contour on cross flow slice at x/D = 6, α = 10°**

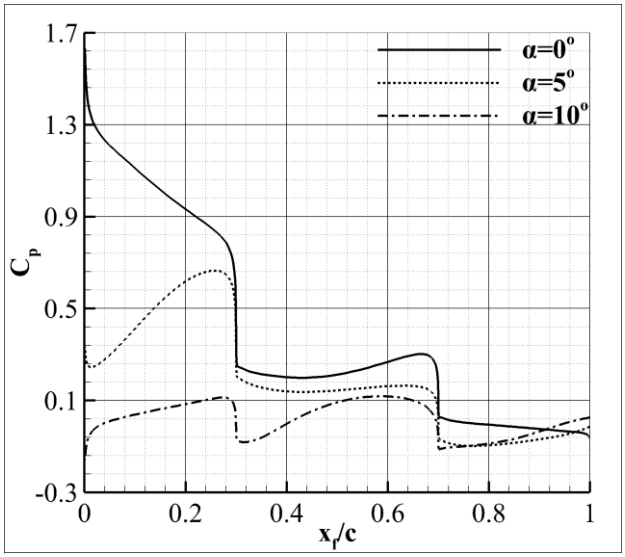


**Fig. 22 Pressure distribution on upper fin surface at $y_f/D$ = 0.5 for finned missile body and shock generator configuration of Δx/D = 0.91, Δy/D = 3.36**

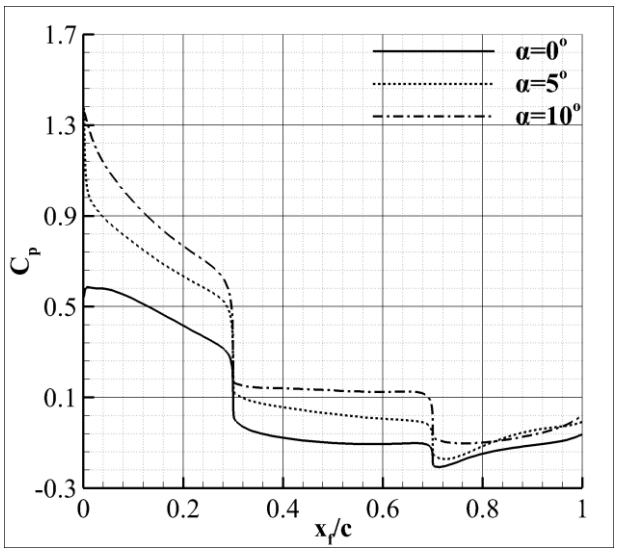


**Fig. 23 Pressure distribution on lower fin surface at $y_f/D$ = 0.5 for finned missile body and shock generator configuration of Δx/D = 0.91, Δy/D = 3.36**

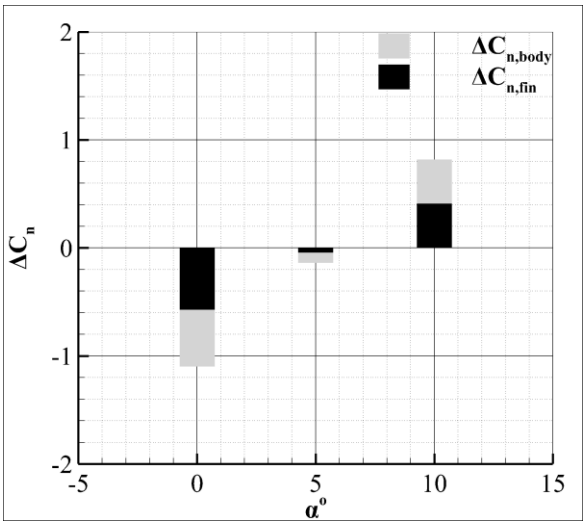


**Fig. 24 Contribution of fins to normal force coefficient of finned missile body for different angles of attack**

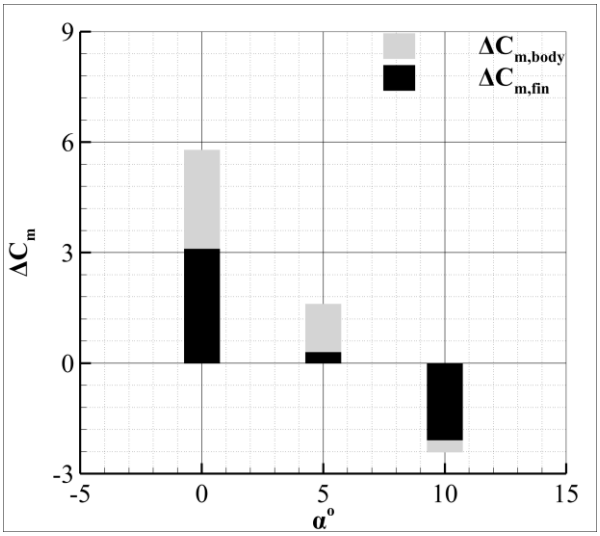


**Fig. 25 Contribution of fins to pitching moment coefficient of finned missile body for different angles of attack**

$0^{\circ}$, which changes to $\Delta C_{p,fin} \approx -1$ for $\alpha = 5^{\circ}$ and $\Delta C_{p,fin} \approx -1.6$ for $\alpha = 10^{\circ}$, as seen in Fig. 22 and Fig. 23. This change in sign convention of normal load acting on the finned missile body tends to pitch down missile as shown in Fig. 24 and Fig. 25. The contribution of interference loads by the fins also gets affected with contribution of body dominating contribution of fin at $\alpha = 5^{\circ}$.

## 4. CONCLUSION

In this work, the effect of shock impingement on aerodynamics of finned missile body has been investigated with the help of computational studies. Firstly, finned missile body were investigated in isolation and the incurred effects of shock impingement on the finned missile body were analysed in comparison to qualitative and quantitative data related to isolated or single body configuration. Axial separation ($\Delta x/D$) between the missile body and shock generator was varied across a region in near vicinity of centre of gravity, keeping lateral separation constant ($\Delta y/D = 3.36$).

The flow field structure between shock generator and missile body consists of impinging shock and expansion waves. A part of impinging shock reflects from the surface of missile and the other part diffracts along the surface of missile. The diffracted shock severely affects the farside flow field ($\Phi \leq 90^{\circ}$) and the expansion waves have less influence on the farside flow field as compared to diffracted shock waves have. Shock impingement induce differential local pressure in comparison to isolated configuration. With increase in angle of attack of missile, there is change in shock structure of both upper inter-fin region and lower inter-fin region due to change in location of shock impingement, which consecutively influences the path of diffracted shock and local flow pitch angles. This causes a change in polarity of forces and moments illustrating extreme sensitivity of missile body to location of shock impingement. The induced loads are due to a combined outcome of local flow pitch ahead of the fin and propagation of shocks and expansion waves. For most configurations, the loads induced by fins are higher than that by body.

## CONFLICT OF INTEREST

The authors have no conflicts of interest.

## AUTHORS CONTRIBUTION

**Mohammed Azhar Ali:** Computational work of all the configurations, writing the manuscript. **Partha Mondal:** Supervision of the computational work, manuscript revision.

## REFERENCES


Alvi, F. S., & Settles, G. S. (1992). Physical model of swept shock wave/boundary layer interaction flowfield, *AIAA Journal*, *30*(9), 2252-2258. https://doi.org/10.2514/3.11212

Ansys (2020). Introduction to Fluent, ANSYS Fluent Theory Manual.

Brosh, A., Kussoy, M. I., & Hung, C. M. (1985). Experimental and numerical investigation of a shock wave impingementon a cylinder. *AIAA Journal*, *23*(6), 840-846. https://doi.org/10.2514/3.8996

Cenko, A., & Waskiewicz, J. (1983). Recent improvements in prediction techniques for supersonic weapon separation. *Journal of Aircraft*, *20*(8), 659-666. https://doi.org/10.2514/3.44926

Chaplin, R., MacManus, D., Leopold, F., Martinez, B., Gauthier, T., & Birch. T. (2011). Computational and experimental investigation into aerodynamic interference between slender bodies in supersonic flow. *Computers & Fluids. 50*, 155–174. https://doi.org/10.1016/j.compfluid.2011.07.009

Dolling, D. S. (2001). Fifty years of shock-wave boundary layer interaction research: what next?, *AIAA Journal*, *39*(8), 1517-1531. https://doi.org/10.2514/2.1476

Gai, S. L., & Teh, S. L. (2000). Interaction between a conical shock wave and a planar oundary layer. *AIAA Journal*, *38*(5), 804-811. https://doi.org/10.2514/2.1060

Ijas Muhammed, V V., Shamsia Banu, N., Suryan, A., Lijo, V., Simurda, D. & Kim, H. D. (2024). Computational study of flow separation in truncated ideal contour nozzles under high-altitude conditions. *International Journal of Fluid Engineering*, *1*, 013101. https://doi.org/10.1063/5.0190399

Jin, Y. & V. Kuznetsov, A. (2024). Multiscale modeling and simulation of turbulent flows in porous media. *International Journal of Fluid Engineering*, 1, 010601. https://doi.org/10.1063/5.0190279

Knight, D. D., Horstman, C. C., Shapey, B., & Bogdonoff, S. (1987). Structure of supersonic turbulent flow past a sharp fin. *AIAA Journal*, *25*(10), 1331-1337. https://doi.org/10.2514/3.9787

Kussoy, M. I., Viegas, J. R., & Horstman, C. C. (1980). Investigation of a three-dimensional shock wave separated boundary layer. *AIAA Journal*, *18*(12), 1477-1484. https://doi.org/10.2514/3.50907

Newman, G., Fulcher, K., Ray, R., & Pinney, M. (1992). *On the aerodynamics/dynamics of store separation from a hypersonic aircraft*. 10th AIAA Applied Aerodynamics Conference, Palo Alto, CA, U.S.A. https://doi.org/10.2514/6.1992-2722

Pickles, J. D., Mettu, B. R., Subbareddy, P. K., & Narayanaswamy, V. (2017). *Sharp-Fin Induced Shock Wave/Turbulent Boundary Layer Interactions in an Axisymmetric Configuration*. 47th AIAA Fluid Dynamics Conference, Denver, Colorado. https://doi.org/10.2514/6.2017-4314 AIAA 2017-4314

Pickles, J. D., Subbareddy, P. K., & Narayanaswamy, V. (2016). *Sharp-Fin Induced Shock Wave/Turbulent Boundary Layer Interactions in an Axisymmetric*

*Configuration*. 46th AIAA Fluid Dynamics Conference, Washington, D.C. https://doi.org/10.2514/6.2016-3340

Pointwise (2019). Pointwise user manual, V18.3, Pointwise, Texas, USA.

Robertson, G., Kumar, R., Eymann, T., & Morton, S. (2015). *Experimental and Numerical Study of Shock-Wave Boundary Layer Interactions on an Axisymmetric Body*. 45th AIAA Fluid Dynamics Conference, Dallas, TX. https://doi.org/10.2514/6.2015-2935

Sawchuk, S. P., & Zamir, M. (1992). Boundary layer on a circular cylinder in axial flow. *International Journal of Heat and Fluid Flow*. *13*(2), 184-188. https://doi.org/10.1016/0142-727X(92)90026-6

Stephen, E., Farnsworth, J. A. N., Porter, C. O., Decker, R., McLaughlin, T., & Dudley, J. G. (2013). *Impinging Shock-Wave Boundary-Layer Interactions on a Three-Dimensional Body*. 43rd AIAA Fluid Dynamics Conference, San Diego, CA. https://doi.org/10.2514/6.2013-2733

Tutty, O. R., Price, W. G., & Parsons, A. T. (2002). Boundary layer flow on a long thin cylinder. *Physics of Fluids*, *14*(2), 628-637. http://dx.doi.org/10.1063/1.1427921

Waskiewicz, J. D., DeJongh, J. E., & Cenko, A. (1983). Application of panel methods to external stores at supersonic speeds. *Journal of Aircraft, 20*(2), 153-158. https://doi.org/10.2514/3.44844

Wilcox, F. J. Jr. (1995). *Separation characteristics of generic stores from lee side of an inclined flat plate at Mach 6.* NASA TM 4652.

Zheltovodov, A. A. (1982). Regimes and properties of three-dimensional separation flows initiated by skewed compression shocks. *Journal of Applied Mechanics and Technical Physics*, *23*(3), 413-418. https://doi.org/10.1007/BF00910085